Journal of Power Sources 192 (2009) 35–42

Contents lists available at ScienceDirect

Journal of Power Sources

journal homepage: www.elsevier.com/locate/jpowsour

Effects of reaction conditions on hydrogen production and carbon nanofiber properties generated by methane decomposition in a fixed bed reactor using a NiCuAl catalyst

I. Suelves [a,*], J.L. Pinilla [a], M.J. Lázaro [a], R. Moliner [a], J.M. Palacios [b]

[a] Instituto de Carboquímica CSIC, Miguel Luesma Castán, 4, 50015 Zaragoza, Spain
[b] Instituto de Catálisis y Petroleoquímica, CSIC, Cantoblanco, Marie Curie 2, 28049 Madrid, Spain

ARTICLE INFO

Article history:
Received 6 October 2008
Received in revised form
21 November 2008
Accepted 22 November 2008
Available online 3 December 2008

Keywords:
Hydrogen production
Carbon nanofiber
Methane decomposition

ABSTRACT

In this paper, the results obtained in the catalytic decomposition of methane in a fixed bed reactor using a NiCuAl catalyst prepared by the fusion method are presented. The influences of reaction temperature and space velocity on hydrogen concentration in the outlet gases, as well as on the properties of the carbon produced, have been investigated. Reaction temperature and the space velocity both increase the reaction rate of methane decomposition, but also cause an increase in the rate of catalyst deactivation. Under the operating conditions used, the carbon product is mainly deposited as nanofibers with textural properties highly correlated with the degree of crystallinity.

1. Introduction

Hydrogen production by means of catalytic decomposition of methane (CDM) into hydrogen and deposited carbon ($CH_4(g) \rightarrow C(s) + 2H_2(g)$) is an interesting alternative to conventional hydrogen production processes, such as steam reforming (SR) and partial oxidation (PO), which result in high CO_2 emissions [1–4].

The carbon properties resulting from CDM are largely dependent on the operating conditions and the type of catalyst used. Methane decomposition using Ni and Ni–Cu catalysts to produce hydrogen and novel carbonaceous materials has been widely reported [5–23]. Activity tests using other transitions metals, such as Fe [24–26] and Co [27,28], have also shown good catalytic performance in CDM.

From these studies, a widely accepted general mechanism of catalyst behaviour and carbon nanofiber formation has been proposed [29,30]. The main steps involved in the CDM process are (i) methane chemisorption on the leading face of a catalyst particle, (ii) dissociation of a chemisorbed CH_4 molecule through progressive breaking of the four C–H bonds, (iii) aggregation of adsorbed atomic hydrogen into molecules, followed by gas phase emission, (iv) atomic carbon aggregation into encapsulated carbon, leading to progressive catalyst deactivation, or atomic carbon diffusion through the bulk catalyst from the leading face to the trailing face, driven by the existing pronounced concentration gradient, and (v) carbon nucleation followed by the formation and growth of carbon nanofibers in the trailing face of the catalyst particle.

In previous works by our research group with nickel-based catalysts, different parameters related to catalyst preparation have been studied. These include the effects of catalyst composition, the presence of Cu as a Ni dopant additive, methods of catalyst preparation [31], the effects of calcination temperatures [32] and the use of different textural promoters [33–35]. From these studies it was concluded that the nickel catalyst prepared by the fusion method using Al_2O_3 as textural promoter and Cu as additive, denoted as NiCuAl with an atomic ratio of 78:6:16, displayed the best performance based on hydrogen production, the amount of carbon deposition as long nanofibers and long catalyst life without deactivation. Furthermore, this simple preparation method, based on a mixture of the respective nitrates, allowed for preparation of catalysts showing similar results to those obtained for catalysts prepared by co-precipitation. The performance of the NiCuAl catalysts in CDM was also assessed in fluidized bed reactor tests, showing the feasibility of this process for the production of large amounts of hydrogen and carbon nanofibers (several hundred grams per day) [36].

Optimization of catalyst performance was achieved in a further study carried out in thermobalance exploring the carbon yields, deposition rates, and changes in the structural properties of the nickel and deposited carbon as a function of the operating temperature and the partial pressures of hydrogen and methane [37].

* Corresponding author. Tel.: +34 976733977; fax: +34 976733318.
E-mail address: isuelves@icb.csic.es (I. Suelves).

0378-7753/$ – see front matter © 2008 Elsevier B.V. All rights reserved.
doi:10.1016/j.jpowsour.2008.11.096

In order to gain a better understanding of NiCuAl catalyst performance, this study focuses on the effects of operating conditions in a fixed bed reactor on hydrogen production and the properties of the deposited carbon. The fixed bed reactor tests allowed for CDM reaction and characterization of the outlet gas after each test by gas chromatography. Despite the extensive methane decomposition literature using nickel catalysts, most studies have been concerned with optimization of catalyst formulation by varying the composition, the type of textural promoter and the additive concentration. Reaction condition studies are less prevalent in spite of the determinant role they play in methane conversion, catalyst deactivation and the resulting properties of the deposited carbon. In order to make the CDM process economically feasible, a complete understanding of these determinant parameters is necessary. Additionally, the structural and morphological properties of the resulting carbon and the textural properties of the samples used are studied for different reaction conditions.

2. Experimental

2.1. Samples

A catalyst, denoted as NiCuAl, with a molar ratio 78:6:16 for the respective components, was prepared using a fusing method. The respective nitric salts of Ni, Cu and Al were mixed to form a powder of the desired composition. This powder was calcined at 350 °C for 1 h to promote thermal decomposition of nitrates into their respective oxides, and subsequently calcined at 450 °C for 8 h. The entire procedure is described in detail elsewhere [31,32].

A detailed characterization study of this fresh catalyst can be found elsewhere [31,32]. The respective powder XRD pattern showed that NiO was the only crystalline phase present in the fresh catalyst with a crystal domain size of 23 nm [37]. According to the literature [20,38], this crystal domain size is suitable to promote carbon deposition as very long nanofibers in a reaction test, providing long-life catalysts in the CDM process. The specific surface area of the fresh calcined catalyst was 80 $m^2\ g^{-1}$, containing mesopores associated with catalyst interparticle voids and supporter of nanometric sizes.

2.2. Experimental setup

Catalytic methane decomposition experiments were carried out in a fixed-bed quartz reactor, 60 cm height, 1.8 cm i.d, heated by an electric furnace. All experiments were conducted at atmospheric pressure.

The study was performed by varying the operating temperature from 550 to 800 °C at a constant weight hourly space velocity (WHSV, defined as the volume of methane fed per hour, per gram of fresh catalyst) of 120 $l\,g_{cat}^{-1}\,h^{-1}$. Additionally, the WHSV was varied from 24 to 1200 $l\,g_{cat}^{-1}\,h^{-1}$ while maintaining a constant temperature of 700 °C.

In a typical test, 50 mg of the fresh catalyst was placed onto wood quartz used as support and a methane flow rate of 20–200 ml min^{-1} was adjusted to obtain the desired WHSV. In tests carried out at higher space velocities, the amount of fresh catalyst was reduced, keeping the available maximum flow rate constant (200 ml min^{-1}) to achieve the required WHSV.

Prior to a CDM experiment, all fresh calcined samples in the oxidised state were subjected to a reduction pre-treatment with a flow rate of 50 ml min^{-1} of pure H_2 at 550 °C for 3 h. The respective powder XRD patterns of samples after the reduction pre-treatment exclusively showed reflections assigned to metallic Ni, the only crystalline phase detected as an active species in the DCM. Further processing of the powder XRD patterns by Rietveld methods revealed that the Ni crystal domain size in the reduced samples was 28 nm, similar to that determined for NiO (23 nm) in the fresh calcined catalysts before the reduction pre-treatment.

The composition of the outlet gas from the reactor was determined by sampling the gas stream with gas bags. The first bag was usually taken some minutes after the CH_4 began flowing and the nitrogen was flushed out, initially present in the reaction system. The gas samples were analysed by means of gas chromatography in a micro GC Varian CP4900 equipped with two packed columns and a TCD detector. In all cases, no methane decomposition products other than hydrogen were detected. The weight of the deposited carbon and the volume of hydrogen produced corresponded, within the experimental error (~5%), to that expected from mass balances, taking into account the stoichiometry of the methane decomposition reaction.

Methane conversion was calculated from the following expression:

$$\chi_{CH_4} = \frac{\%H_2}{200 - \%H_2} \quad (1)$$

Carbon deposition rate (r_C) was calculated from the carbon balance among the methane fed into the reactor and the methane reacted, according to the stoichiometry of the methane decomposition reaction.

2.3. Characterization techniques

The textural properties of the fresh and used samples were measured by N_2 adsorption at 77 K in a Micromeritics ASAP2020 apparatus. The specific surface areas and pore volumes were calculated by applying the BET method to the respective N_2 adsorption isotherms.

Powder X-ray diffraction (XRD) patterns of fresh and used samples were acquired in a PANalytical diffractometer using a θ–2θ configuration, Ni-filtered Cu Kα radiation and a secondary graphite monochromator. The angle range scanned was 10–100° using a counting step of 0.02° and a counting time per step of 20 s. A suitable sample holder with a very low noise level was used, allowing for pattern acquisitions from a small amount of sample with good resolution. The powder XRD patterns were further processed using the accompanying X'Pert Highscore Plus software to obtain refined structural parameters for the desired compounds through the application of Rietveld methods.

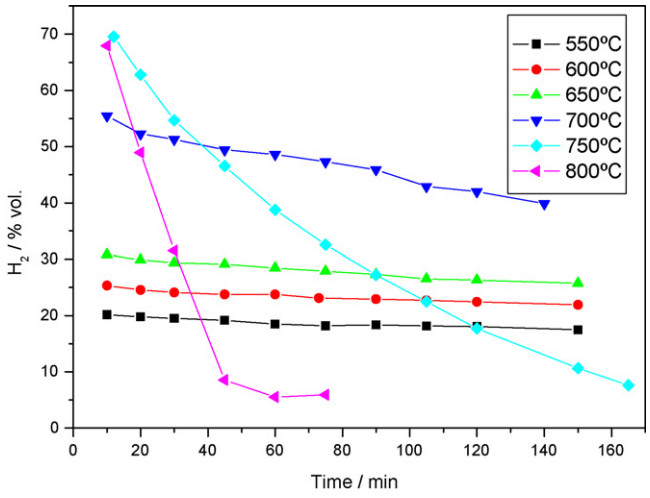

Fig. 1. Influence of reaction temperature on the evolution of hydrogen concentration. WHSV: 120 $l\,g_{cat}^{-1}\,h^{-1}$.

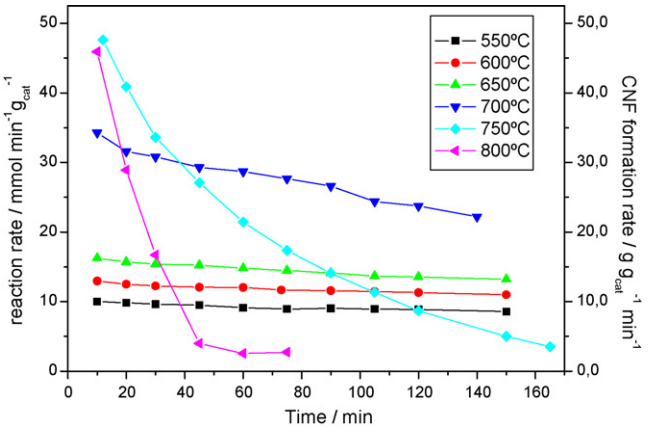

Fig. 2. Influence of reaction temperature on the evolution of methane decomposition rate and carbon formation rate. WHSV: 120 l g_{cat}^{-1} h^{-1}.

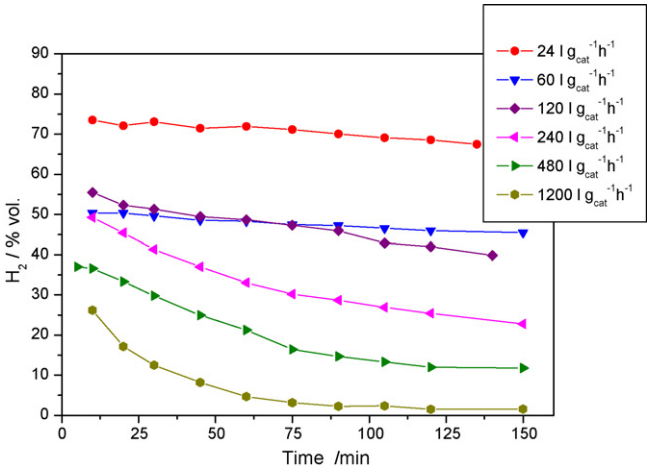

Fig. 3. Influence of space velocity on the evolution of hydrogen concentration T = 700 °C.

The morphological appearance of the deposited carbon was studied with an electron microscope (SEM) (Hitachi S-3400) coupled to a Si/Li detector for energy dispersive X-ray (EDX) analysis.

3. Results

3.1. Activity tests

3.1.1. Influence of reaction temperature

The effect of the reaction temperature in the tests carried out using the NiCuAl catalyst at a WHSV of 120 l g_{cat}^{-1} h^{-1} is shown in Fig. 1. At low reaction temperatures, that is, 550, 600 and 650 °C, low hydrogen concentrations of 20, 26 and 31 vol%, respectively, were measured in the outlet gas. However, these concentrations were kept constant throughout the test, indicating that the catalyst maintained its initial activity during the entire run without apparent deactivation. The tests performed at higher temperatures revealed that, the initial hydrogen concentrations were much higher, 55, 67 and 70 vol% at 700, 750 and 800 °C, respectively, as expected from thermal activation. However, the evolving hydrogen concentrations dropped quickly, indicating rapid catalyst deactivation. This effect was more evident as reaction temperature increased. For instance, in the tests carried out at 750 and 800 °C, hydrogen concentration dropped to values lower than 5 vol% in 160 and 60 min, respectively.

Similarly, the effect of the reaction temperature on the methane decomposition rate and the carbon deposition rate is shown in Fig. 2. The shape of the curves follow the same pattern as those in Fig. 1, revealing that a rise in the reaction temperature increases the initial reaction rate while increasing the catalyst deactivation rate.

Table 1 summarizes the results obtained at different reaction temperatures, including some parameters extracted from the experiments: the initial methane decomposition rate, r_{CH_4}; the average methane conversion, X_{CH_4}; the thermodynamic methane conversion, $(X_{CH_4})_{eq}$; the total carbon deposited per gram of catalyst loaded, C_{dep}; and the carbon deposition rate, r_C. It can be observed that the average methane conversion, X_{CH_4}, shows a maximum of 31.2% at 700 °C. The amount of carbon deposited at 700 °C after 150 min of reaction time was 46.8 g g_{cat}^{-1}, noting that the catalyst testing could go on for several more hours before reaching complete catalyst deactivation.

The effect of the reaction temperature on the performance of metallic catalysts used in methane decomposition is well illustrated in the literature [10,14–16,19,37,39], and is widely considered the most relevant parameter in catalyst deactivation. In a previous study [37], it was concluded that catalyst deactivation of Ni, operating at a high temperature (800 °C) in a differential reactor, was due to thermal sintering of Ni particles. In this study, powder XRD patterns (not shown) taken from used catalysts showed nickel domain sizes of 34 nm in samples used at 550 °C. This is very similar to those of the 36 nm samples obtained in tests carried out at 800 °C. These results imply that thermal sintering of Ni is not responsible for catalyst deactivation during the tests carried out in the fixed bed reactor, given that the hydrogen produced during reaction may prevent Ni sintering. According to the study mentioned [37], the increase in hydrogen partial pressure might prevent thermal sintering of catalyst through a decrease in the surface energy of Ni by H_2 adsorption. In this study, has been found that the only cause of catalyst deactivation at high temperatures is the formation of a more ordered carbon, as revealed by measurements of structural and textural properties of the deposited carbon as discussed below.

3.1.2. Influence of space velocity

The evolution of the hydrogen concentration in the outlet gases from the reactor at different space velocities, 24–1200 l g_{cat}^{-1} h^{-1}, at 700 °C is shown in Fig. 3. Increasing the space velocity has two clear effects: the hydrogen concentration in the outlet gases diminishes, and the catalyst deactivation substantially increases. These effects have been shown in previous studies [9,23,40]. For example,

Table 1
Summary of the main parameter obtained in the experiments at different temperatures (VS: 120 l g_{cat}^{-1} h^{-1}).

T (°C)	$r_{CH_{4,o}}$ (mmol min^{-1} g_{cat}^{-1})	$(X_{CH_4})_{eq}$ (%)	X_{CH_4} (%)	C_{dep} (g g_{cat}^{-1})	r_C (gC g_{cat}^{-1} h^{-1})
550	10.02	34	10.20	16.4	6.56
600	12.96	52.1	13.19	21.3	8.51
650	16.25	64.2	16.17	26	10.40
700	34.27	79.3	31.20	46.8	20.06
750	47.60	85	22.06	39[a]	14.18
800	45.95	91.5	19.41	15.6[a]	16.22

[a] Catalyst deactivated.

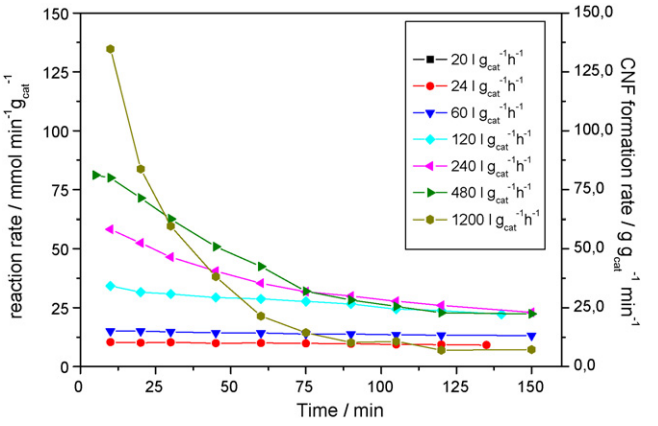

Fig. 4. Influence of space velocity in the evolution of methane decomposition rate and carbon formation rate. T = 700 °C.

at a low spatial velocity of 24 l g_{cat}^{-1} h^{-1}, the initial hydrogen concentration was about 75 vol%, close to thermodynamic equilibrium concentration at this temperature. In other works using a NiCuAl catalyst at a low space velocity of 4 l g_{cat}^{-1} h^{-1}, a constant hydrogen concentration of 80 vol% was found for an 8 h run time [31]. The experiments carried out at space velocities in the 20–60 l g_{cat}^{-1} h^{-1} range still showed high stability in the evolving hydrogen concentration. However, as the space velocity was further increased over 120–1200 l g_{cat}^{-1} h^{-1}, the curve shape changed dramatically, showing a progressive reduction in the hydrogen concentration with reaction time. This continued to a low-value of almost constant methane conversion until the end of the run. For example, at 1200 l g_{cat}^{-1} h^{-1}, the catalyst became fully deactivated showing hydrogen concentrations lower than 5% after 60 min.

In order to gain a deeper understanding of the effect of the space velocity, the evolution of methane decomposition and carbon production rates have been plotted in Fig. 4. Despite the fact that the increase in the space velocity reduces the hydrogen concentration in the outlet gas, it is worth noting that the initial reaction rate increased significantly, from 10.34 mmol min^{-1} g_{cat}^{-1} at a space velocity of 24 l g_{cat}^{-1} h^{-1} to 135 mmol min^{-1} g_{cat}^{-1} at the highest space velocity of 1200 l g_{cat}^{-1} h^{-1}.

Table 2 summarizes the obtained results, including some kinetic data for the methane decomposition at space velocities of 24–1200 l g_{cat}^{-1} h^{-1} using the NiCuAl catalyst. It can be observed that the initial reaction rate and the average methane conversion move in opposite directions. The greatest total amounts of deposited carbon, obtained before the catalyst became completely deactivated, occurred at space velocities of 480 and 1200 l g_{cat}^{-1} h^{-1} with carbon depositions of 84 and 141 g g_{cat}^{-1}, respectively.

From the above results it can be concluded that the methane decomposition is highly dependent on the operating temperature and on the space velocity. These variables also substantially affect the catalyst deactivation rate. High space velocities also maximize the amount of deposited carbon, up to 141 g g_{cat}^{-1} in 60 min at a space velocity of 1200 l g_{cat}^{-1} h^{-1}.

Table 2
Summary of the main parameter obtained in the experiments at different space velocity (T: 700 °C).

WHVS (l g_{cat}^{-1} h^{-1})	r_o (mmol min^{-1} g_{cat}^{-1})	X_{CH_4} (%)	C_{dep} (g g_{cat}^{-1})	r_C (g g_{cat}^{-1} h^{-1})
24	10.38	54.61	15.8	7.02
60	15.01	31.36	39	15.60
120	34.27	31.2	46.8	20.06
240	58.31	20.09	64.6	25.84
480	79.95	11.63	84[a]	33.60
1200	134.74	8.77	141[a]	56.40

[a] Catalyst deactivated.

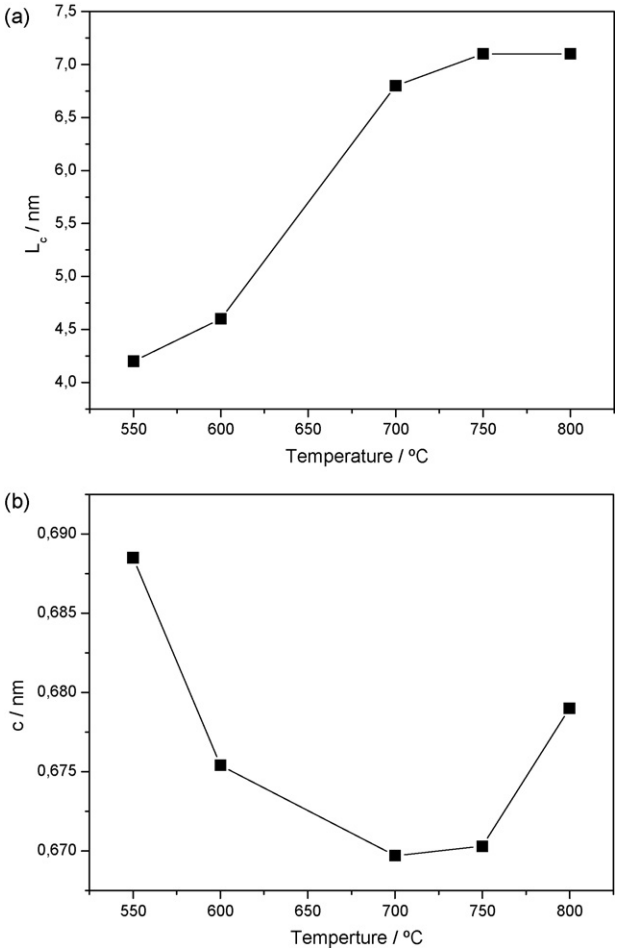

Fig. 5. Variation of crystal domain size (a) and parameter c of the hexagonal unit cell (b) of the deposited carbon with operating temperature.

3.2. Characterization of the deposited carbon in used catalysts

3.2.1. Structural parameters and crystallinity

The structural properties of the deposited carbon in used samples were studied through the calculation of the average crystal domain size, L_c, along a direction perpendicular to the basal planes in a graphitic-type structure, and the respective parameter, c, of the hexagonal cell. The variation of both parameters with operating temperature is shown in Fig. 5a and b. The crystal domain size, L_c, increased, first, with the operating temperature until reaching a nearly constant value at temperatures higher than 750 °C. These results are in agreement with those found in a previous work carried out with a thermobalance, in which it was concluded that the deposited carbon from methane decomposition became more ordered at higher operating temperatures [37].

Additionally, the variation of the parameter, c, of the hexagonal unit cell of the deposited carbon, is shown in Fig. 5b. The parameter c decreased from a value of 0.6857 nm at 550 °C to a value of 0.6704 at 750 °C. Taking into account the fact that c is equal to 0.6704 nm for a perfect graphite, it can be deduced that the parameter c of the deposited carbon is highly dependent on the reaction temperature, going from a highly turbostratic carbon at low temperatures to a more graphitic carbon at high temperatures.

Crystallinity and interplanar spaces data indicate that at low operating temperatures carbon was deposited as highly disordered

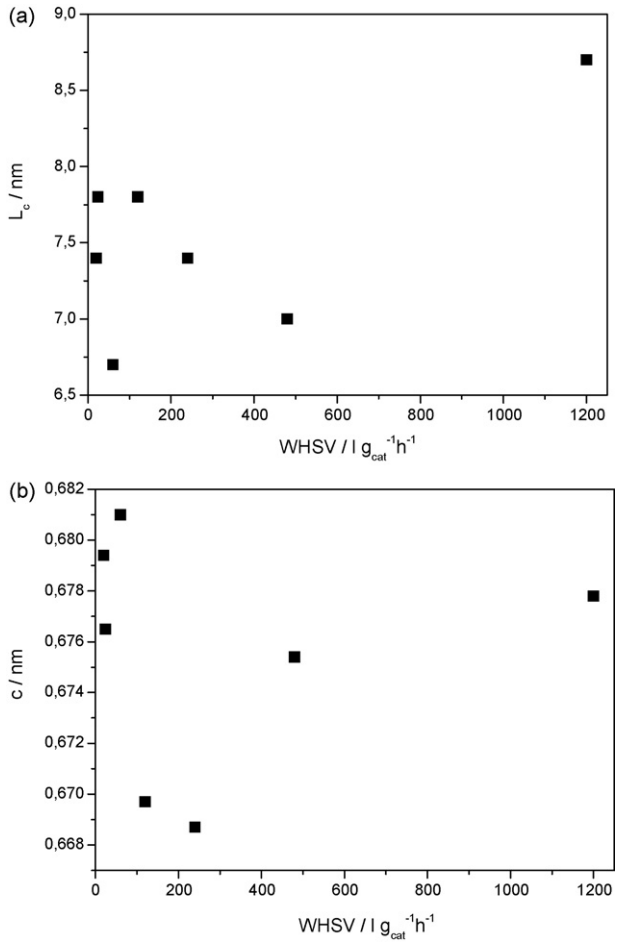

Fig. 6. Variation of crystal domain size (a) and parameter *c* of the hexagonal unit cell (b) of the deposited carbon with space velocity.

carbon, usually as long nanofibers emerging from Ni particles, promoting a long-life catalyst. At high operating temperatures, however, carbon was deposited as a well-ordered, almost graphitic carbon, usually associated with coatings of uniform thickness on Ni particles, leading to fast catalyst deactivation.

Similar effects of the space velocity on the crystal domain size, L_c, and on the parameter, *c*, of the hexagonal unit cell of the deposited carbon are shown in Fig. 6a and b, respectively. According to data in the literature the main effect of the space velocity, presumably, could be derived from the changes in the hydrogen partial pressure. However, the plots shown in Fig. 6 reveal that the effect of the space velocity on the structural properties of the deposited carbon is not clear. The crystal domain size, L_c, (Fig. 6a) of the deposited carbon takes values that range from 6.7 to 7.8 nm. The highest value, however, was obtained at the highest space velocity. Similarly, the variation of the parameter, *c*, shown in Fig. 6b is also inconsistent,

Table 3
Textural parameters obtained by N_2 adsorption.

Conditions	S_{BET} ($m^2\ g^{-1}$)	S_{meso} ($m^2\ g^{-1}$)	S_{micro} ($m^2\ g^{-1}$)	V_p ($cm^3\ g^{-1}$)
Temperature (°C) (VS: 120 l $g_{cat}^{-1}\ h^{-1}$)				
550	135	116	19	0.39
600	146	127	18	0.38
650	134	117	17	0.34
700	110	99	11	0.29
750	130	123	7	0.25
800	93	89	4	0.23
WHSV (l $g_{cat}^{-1}\ h^{-1}$) (*T*: 700 °C)				
24	93	84	9	0.26
60	116	103	13	0.27
120	110	99	11	0.29
240	121	111	10	0.31
480	142	131	11	0.38
1200	118	112	6	0.29

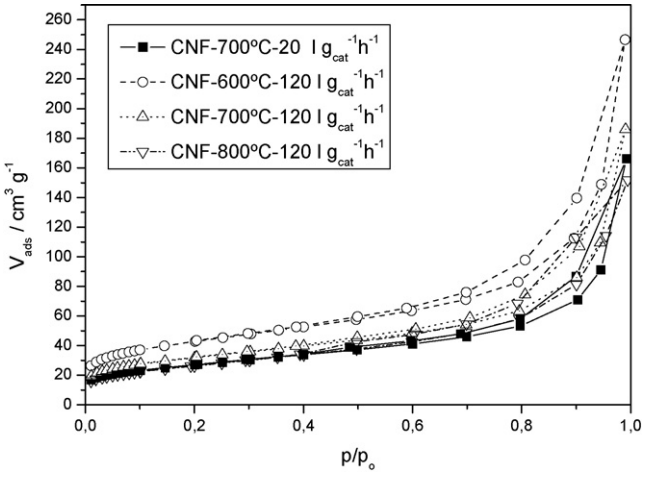

Fig. 7. N_2 adsorption isotherms of the used samples at different temperatures and space velocities.

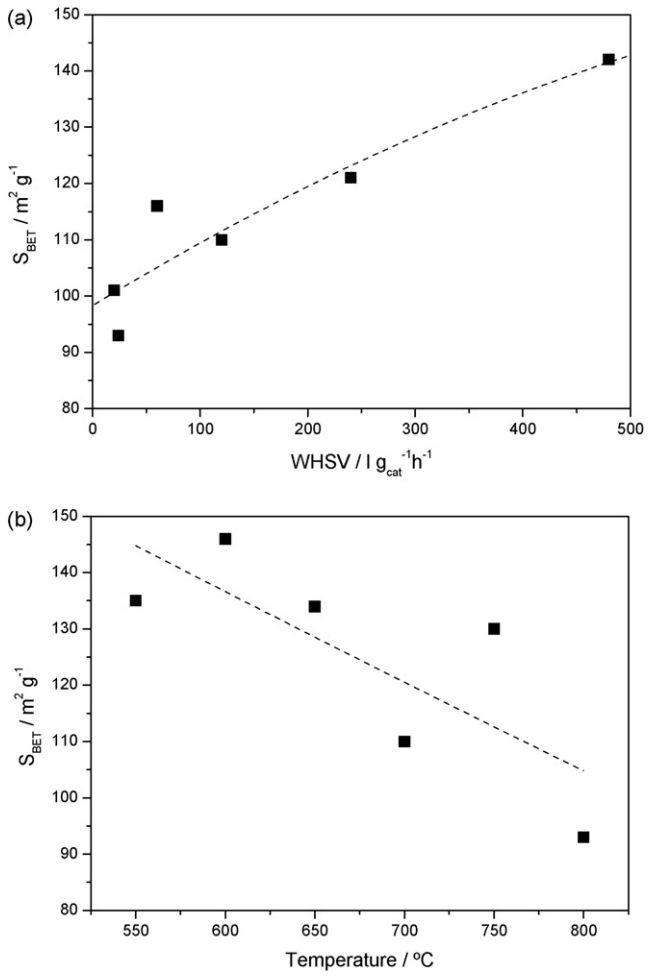

Fig. 8. Variation of the specific surface area of used samples with the space velocity (a) and reaction temperature (b).

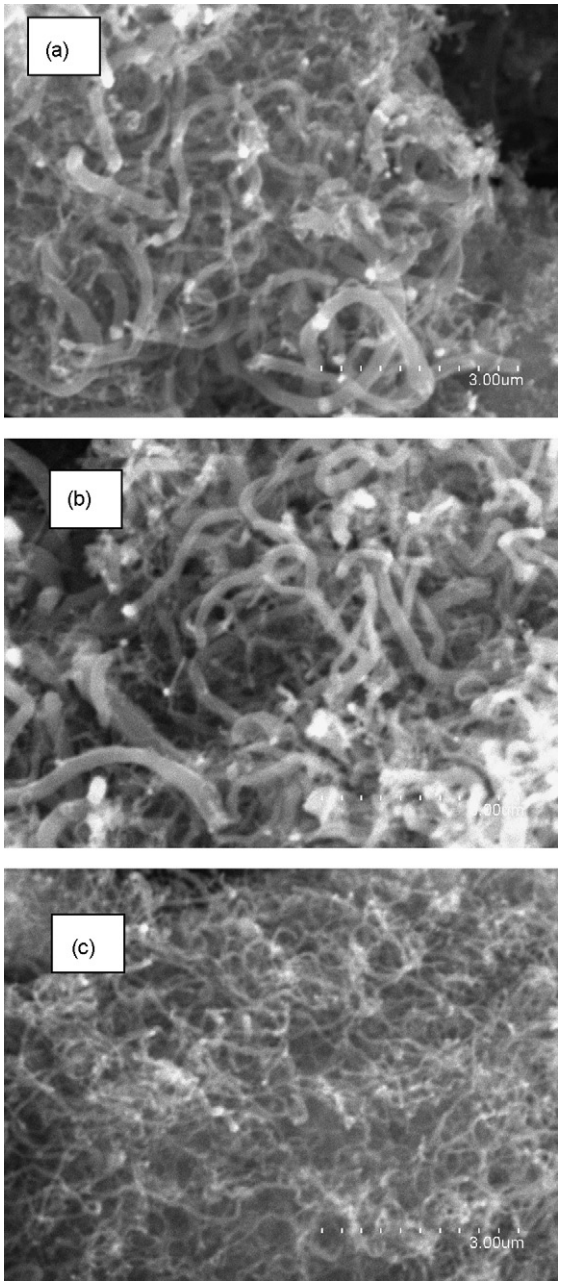

Fig. 9. SEM micrographs of used catalyst NiCuAl tested at different reaction temperatures: 600 °C (a); 700 °C (b); 800 °C (c).

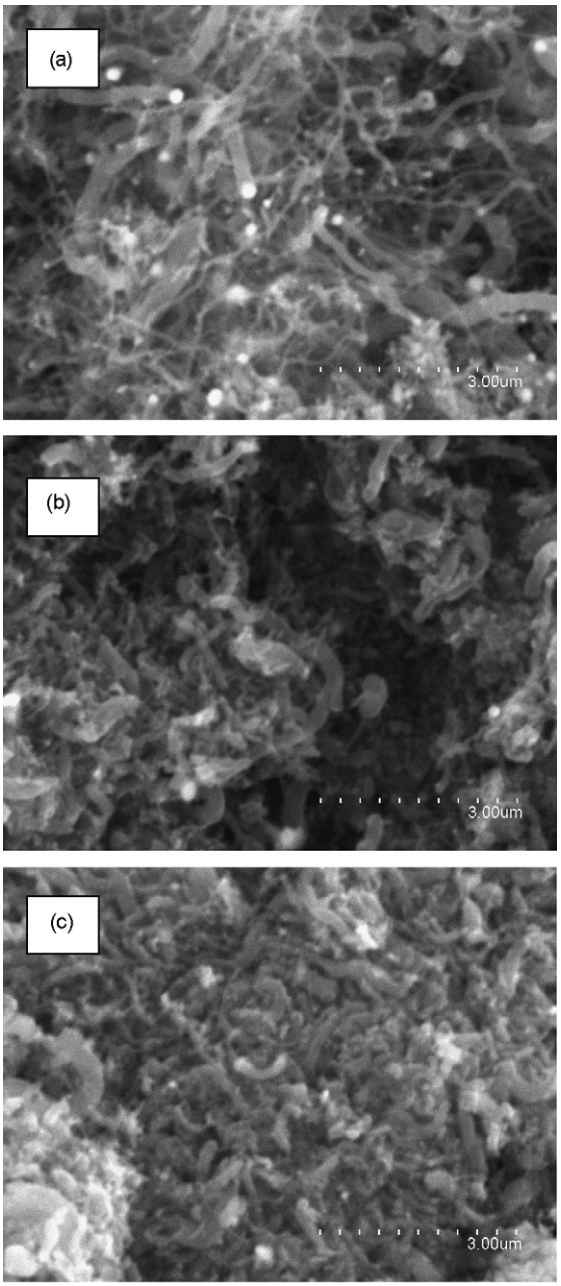

Fig. 10. SEM micrographs of used catalyst NiCuAl tested at different space velocities: 20 $l g_{cat}^{-1} h^{-1}$ (a); 240 (b); 480 $l g_{cat}^{-1} h^{-1}$ (c).

but the values obtained at the highest space velocities correspond to nearly graphitic carbons.

From the results of the XRD study, it can be concluded that the reaction temperature has a clear effect on the structural properties of the deposited carbon; however, this effect is unclear in the case of spatial velocities. Additional measurements of textural properties and SEM studies, discussed below, may help in gaining a clearer understanding.

3.2.2. Measurement of textural properties

The catalysts tested at different reaction temperatures and space velocities were also characterized by means of N_2 adsorption at 77 K. Some typical isotherms of the used samples at different operating conditions, shown in Fig. 7, can be clearly assigned to the type IV IUPAC classification, characteristic of mesoporous materials. Additionally, these isotherms present an H3-type hysteresis loop, commonly related to capillary condensation in laminar mesopores [41]. Given that the used materials had a carbon content higher than 90 wt%, the studied textural properties are almost exclusively due to the deposited carbon and not to the fresh catalyst. The textural parameters obtained by applying the BET equation to the respective isotherms are shown in Table 3, including the total specific surface area and its distribution between mesopore and micropore surface areas, and the total pore volume. The specific surface area of used samples show values ranging from 93 to 146 $m^2 g^{-1}$, higher than those found in the fresh sample (80 $m^2 g^{-1}$), in both cases assigned to the presence of mesopores. In the case of the fresh samples, the specific surface area was assigned to interparticle voids between nanometric catalyst particles and the support; however, in the case of the used samples, they are mostly due to the presence of carbon nanofibers with mesopores mostly located in the interior of

Table 4
Literature comparison of some Ni–Cu based catalyst in the CDM.

Reference	Catalyst	T (°C)	m_{cat} (g)	Flow rate (N cm^3 min^{-1})	WHSV (l g_{cat}^{-1} min^{-1})	C_{dep} (gC g_{cat}^{-1})	t (h)	r_C (gC g_{cat}^{-1} h^{-1})
[15]	75Ni–15Cu–Al_2O_3	675	0.1	150	90	404	27.5	14.69
[15]	82Ni–8Cu–Al_2O_3	675	0.1	150	90	150	9	16.67
[15]	62Ni–25Cu–Al_2O_3	675	0.1	150	90	293	20	14.65
[16]	15Ni–3Cu–2Al	700	0.1	68	40.8	280	32.5	8.62
[17]	NiCuMg (2.4:0.6:1)	700	0.05	60	72	420	33	12.73
[17]	NiCuMg (2.4:0.6:1)	725	0.05	60	72	262.8	19	13.83
[17]	NiCuMg (2.4:0.6:1)	750	0.05	60	72	166.8	11	15.16
[18]	65Ni25Cu10Nb_2O_5	700	0.050		48	284	32	8.9
This work	NiCuAl (78:6:16)	700	0.05	100	120	39	2.75	14.18
This work	NiCuAl (78:6:16)	700	0.01	200	1200	141	1	141

the nanofibers along the fiber axis, as discussed below in the SEM study.

In order to elucidate the influence of the two studied variables on the textural properties, the specific surface area of used samples is plotted versus the space velocity and the reaction temperature in Fig. 8a and b, respectively. It is observed that as the operating temperature increases, the specific surface area of the deposited carbon decreases, in agreement with the results obtained by others authors [15,42]. An opposite trend is found as the specific surface area increases with the space velocity. The total pore volume takes values ranging from 0.23 to 0.39 cm^3 g^{-1}, showing a similar trend between the operating temperature and space velocity as that for specific surface area.

Low specific surface areas of carbonaceous materials are typically assigned to highly ordered graphitic carbon while high specific surface areas are associated with highly disordered carbons. Thus, from the study of the textural properties of the used samples, it is concluded that the effect of the reaction temperature on the textural properties is in agreement with the XRD study but in disagreement with the effect of the spatial velocity, in which case a decrease in the specific surface area was expected. Additional SEM studies are performed to further study the effect of the spatial velocity.

3.2.3. Morphological studies of the used samples

SEM micrographs of the used samples reveal that the deposited carbon usually appears as nanofilaments emerging from very bright nickel catalyst particles. Three representative micrographs obtained at three different reaction temperatures, 600, 700 and 800 °C, are shown in Fig. 9. The sample obtained at 600 °C (Fig. 9a) displays many bright spots, due to Ni particles, located at the tip of the growing carbon nanofibers. As the temperature increases the presence of bright spots becomes much less evidenced, although the diameter of the carbon nanofibers is similar in both samples at 600 and 700 °C (Fig. 9b). The SEM image of the sample obtained at 800 °C (Fig. 9c) reveals the presence of much thinner carbon nanofilaments. Since the nanofibers in this sample were formed during the first stages of the test, in the presence of high hydrogen partial pressure, it can prevent Ni thermal sintering and, consequently, the enlargement of carbon nanofibers.

The effect of space velocity on the morphological appearance of the deposited carbon at 24, 240 and 480 l g_{cat}^{-1} h^{-1} is shown in Fig. 10a–c, respectively. As the space velocity increases, the presence of Ni particles at the tip of the growing nanofibers are less visible and the samples appear much denser due to the larger amount of deposited carbon (Table 2), but no differential morphological features are apparent.

3.3. NiCuAl catalyst performance

The NiCuAl catalyst in this study showed good performance in CDM in terms of carbon deposition. The best performance of NiCu catalysts reported in the literature were obtained at temperatures around 600 °C. For example, Reshetenko et al. [15] reported carbon depositions of 525 g g_{cat}^{-1} at 625 °C. Other authors obtained ca. 200 g g_{cat}^{-1} [13] at 500 °C and 380 g g_{cat}^{-1} at 600 °C [16]. It also worth noting that these carbon depositions were achieved at catalyst lifetimes higher than 50 h. The possible use of temperatures greater than 650 °C is very interesting because of the rapid increase in methane conversion [15,17]. However, the fast catalyst deactivation at temperatures higher than 700 °C is a drawback. Thus, it is worthwhile to develop active catalysts that are suitable to be tested at higher temperatures, prevent deactivation, and allow carbon nanofiber formation, key for avoiding catalyst encapsulation. Recently, the use of Fe catalysts have been reported to withstand higher temperatures [26,43], although methane decomposition rates are much lower in comparison to those of nickel.

It should also be noted that from the studies published in the literature dealing with methane decomposition several different space velocity conditions are reported, which makes catalyst performance comparisons difficult. Additionally, the use of diluted methane in different concentrations introduces another parameter that has to be taken into account. As an example, there has been a recent report [40], in which the amount of catalyst used along with the methane flow rate and methane concentration used are presented, showing a wide range of weight space velocities, ranging from 1 to 72 l g_{cat}^{-1} h^{-1}.

In an attempt to compare the NiCuAl performance used in the present work, some results available in the literature for massive NiCu catalyst, in terms of carbon capacity, are shown in Table 4. For the catalyst selected, the methane decomposition reaction was carried out using undiluted methane at relative high temperatures (around 700 °C). Additionally, test conditions (catalyst mass, methane flow rate and WHSV), as well as run time and the average carbon deposition rate, expressed in grams of carbon per gram of catalyst and per hour, are also included.

From the results reported in the literature, high carbon capacious catalyst have been reported (up to 404 g g_{cat}^{-1} at 675 °C [15]) using reaction times from 9 to 30 h. The catalyst tested in this work, shows a carbon capacity lower than the others reported in the literature, 141 g g_{cat}^{-1}. However, the reaction time is much lower, just 1 h, which clearly indicates the faster carbon formation rate performed by the NiCuAl catalyst at 700 °C.

4. Conclusions

An increase in the operating temperature and space velocity enhances the methane reaction rate but also leads to faster catalyst deactivation. By increasing the operating temperature formation of more ordered deposited carbon is promoted, likely explaining the rapid catalyst deactivation. In the case of the spatial velocity the process of catalyst deactivation is not as clear. However, it does not seem to be associated with structural changes of the deposited car-

bon but, rather, to the great amount of accumulated carbon in the used sample.

Acknowledgements

This work was carried out with financial support from the Spanish CDTI (Project CENIT SPHERA), GAS NATURAL, S.A and the Spanish MEC (Proyecto ENE2005-03801 Plan Nacional de Energía-FEDER).

References

[1] D. Hart, P. Freud, A. Smith, Hydrogen Today and Tomorrow, IEA GHG Programme, April 1999. ISBN 1 898373248.
[2] CO_2 Abatement by the use of Carbon-Rejection Processes, IEA GHG Report PH3/36 February 2001.
[3] M. Steinberg, Int. J. Hydrogen Energy 23 (1998) 419–425.
[4] N.Z. Muradov, Energy Fuels 12 (1998) 41–48.
[5] S.K. Shaikhutdinov, L.B. Avdeeva, O.V. Goncharova, D.I. Kochubey, B.N. Novgorodov, L.M. Plyasova, Appl. Catal. A: Gen. 126 (1995) 125–139.
[6] V.B. Fenelonov, Ayu. Derevyankin, Lg. Okkel, L.B. Avdeeva, V.I. Zaikovskii, E.M. Moroz, A.N. Salanov, N.A. Rudina, V.A. Likholobov, Carbon 35 (1997) 1129–1140.
[7] G.G. Kuvshinov, Mogilnykh Yu.I, D.G. Kuvshinov, V.I. Zaikovskii, L.B. Avdeeva, Carbon 36 (1998) 87–97.
[8] Y. Li, J. Chen, L. Chang, Y. Qin, J. Catal. 178 (1998) 76–83.
[9] Y. Li, J. Chen, Y. Qin, L. Chang, Energy Fuels 14 (6) (2000) 1188–1194.
[10] M.A. Ermakova, D.Y. Ermakov, G.G. Kuvshinov, Appl. Catal. A: Gen. 201 (2000) 61–70.
[11] T.V. Choudhary, C. Sivadinarayana, C.C. Chusuei, A. Klinghoffer, D.W. Goodman, J. Catal. 199 (2001) 9–18.
[12] P. Wang, E. Tanabe, K. Ito, J. Jia, H. Morioka, T. Shishido, K. Takehira, Appl. Catal. A: Gen. 231 (2002) 35–44.
[13] S. Takenaka, S. Kobayashi, H. Ogihara, K. Otsuka, J. Catal. 217 (2003) 79–87.
[14] J.I. Villacampa, C. Royo, E. Romeo, J.A. Montoya, P. Del Angel, A. Monzón, Appl. Catal. A: Gen. 252 (2003) 363–383.
[15] T.V. Reshetenko, L.B. Avdeeva, Z.R. Ismagilov, A.L. Chuvilin, V.A. Ushakov, Appl. Catal. A: Gen. 247 (July (1)) (2003) 51–63.
[16] J. Chen, Y. Li, Z. Li, X. Zhang, Appl. Catal. A: Gen. 269 (August (1–2)) (2004) 179–186.
[17] H. Wang, R.T.K. Baker, J. Phys. Chem. B. 108 (52) (2004) 20273–20277 (article).
[18] J. Li, G. Lu, K. Li, W. Wang, J. Mol. Catal. A: Chem. 221 (November (1–2)) (2004) 105–112.
[19] I. Suelves, M.J. Lázaro, R. Moliner, B.M. Corbella, J.M. Palacios, Int. J. Hydrogen Energy 30 (2005) 1555–1567.
[20] D. Chen, K.O. Christensen, E. Ochoa-Fernández, Z. Yu, B. Totdal, N. Latore, A. Monzón, A. Holmen, J. Catal. 229 (2005) 82–96.
[21] A. Venugopal, S. Naveen Kumar, J. Ashok, D. Hari Prasad, V. Durga Kumari, K.B.S. Prasad, M. Subrahmanyam, Int. J. Hydrogen Energy 32 (August (12)) (2007) 1782–1788.
[22] J. Ashok, S. Naveen Kumar, A. Venugopal, V. Durga Kumari, M. Subrahmanyam, J. Power Sources 164 (February (2)) (2007) 809–814.
[23] I. Kvande, D. Chen, Z. Yu, M. Rønning, A. Holmen, J. Catal. 256 (June (2)) (2008) 204–214.
[24] M.A. Ermakova, D.Y. Ermakov, A.L. Chuvilin, G.G. Kuvshinov, J. Catal. 201 (2001) 183–197.
[25] L.B. Avdeeva, T.V. Reshetenko, Z.R. Ismagilov, V.A. Likholobov, Appl. Catal. A: Gen. 228 (2002) 53–63.
[26] S. Takenaka, M. Serizawa, K. Otsuka, J. Catal. 222 (2004) 520–531.
[27] H.Y. Wang, E. Ruckenstein, Carbon 40 (2002) 1911–1917.
[28] Y. Zhang, K.J. Smith, Catal. Today 77 (2002) 257–268.
[29] S.G. Zavarukhin, G. Kuvshinov, Appl. Catal. A: Gen. 272 (2004) 219–227.
[30] Y. Zhang, K.J. Smith, J. Catal. 231 (2005) 354–364.
[31] I. Suelves, M.J. Lázaro, R. Moliner, Y. Echegoyen, J.M. Palacios, Catal. Today 116 (2006) 271–280.
[32] Y. Echegoyen, I. Suelves, M.J. Lázaro, R. Moliner, J.M. Palacios, J. Power Sources 169 (June (1)) (2007) 150–157.
[33] M.J. Lázaro, Y. Echegoyen, I. Suelves, J.M. Palacios, R. Moliner, Appl. Catal. A: Gen. 329 (October) (2007) 2–29.
[34] Y. Echegoyen, I. Suelves, M.J. Lázaro, M.L. Sanjuán, R. Moliner, Appl. Catal. A: Gen. 333 (December (2)) (2007) 229–237.
[35] M.J. Lázaro, Y. Echegoyen, C. Alegre, I. Suelves, R. Moliner, J.M. Palacios, Int. J. Hydrogen Energy 33 (July (13)) (2008) 3320–3329.
[36] J.L. Pinilla, R. Moliner, I. Suelves, M.J. Lázaro, Y. Echegoyen, J.M. Palacios, Int. J. Hydrogen Energy 32 (2007) 4821–4829.
[37] J.L. Pinilla, I. Suelves, M.J. Lázaro, R. Moliner, J.M. Palacios, Int. J. Hydrogen Energy 33 (May (10)) (2008) 2515–2524.
[38] K. Otsuka, H. Ogihara, S. Takenaka, Carbon 41 (February (2)) (2003) 223–233.
[39] J. Chen, Y. Qiao, Y. Li, Appl. Catal. A: Gen. 337 (March (2)) (2008) 148–154.
[40] A.F. Cunha, J.J.M. Órfão, J.L. Figueiredo, Appl. Catal. A: Gen. 348 (2008) 103–112.
[41] K.S.W. Sing, D.H. Everett, R.A.W. Haul, L. Moscov, R.A. Pierotti, J. Rouquérol, T. Siemieniewska, Pure Appl. Chem. 57 (1985) 603–619.
[42] T.V. Reshetenko, L.B. Avdeeva, Z.R. Ismagilov, V.V. Pushkarev, S.V. Cherepanova, A.L. Chuvilin, V.A. Likholobov, Carbon 41 (8) (2003) 1605–1615.
[43] A. Konieczny, K. Mondal, T. Wiltowski, P. Dydo, Int. J. Hydrogen Energy 33 (January (1)) (2008) 264–272.